Measurements of germanium *K*-shell ionization cross sections and tin *L*-shell x-ray production cross sections by electron impact

Changhuan Tang[a)]
National Key Laboratory of Laser Fusion, Research Center of Laser Fusion, China Academy of Engineering Physics, P.O. Box 919-986, Mianyang, Sichuan 621900, People's Republic of China and Key Laboratory for Radiation Physics and Technology of Education Ministry of China, Institute of Nuclear Science and Technology, Sichuan University, Chengdu 610064, People's Republic of China

Zhu An, Zhengming Luo, and Mantian Liu
Key Laboratory for Radiation Physics and Technology of Education Ministry of China, Institute of Nuclear Science and Technology, Sichuan University, Chengdu 610064, People's Republic of China

(Received 27 August 2001; accepted for publication 25 February 2002)

This article reports experimental measurements of germanium *K*-shell ionization cross sections and tin *L*-shell x-ray production cross sections by electron impact. In order to avoid the difficulty of preparing thin and uniform self-supporting targets, thin targets with thick substrates are used in the experiments. Since electrons reflected by the substrate can induce additional ionization of target atoms, we developed a method to correct the measured x-ray intensities and eliminated the influence of the substrate on measured data. Our measured cross sections are in good agreement with previous measurements. The present results are also compared with the predictions of theories and semiempirical and empirical formulas. It is found that the *K*-shell ionization cross sections of Ge at energies from near threshold to 40 keV can be reasonably described by the semiempirical formula of Green and Cosslett. Experimental absolute *L*-shell x-ray production cross sections of Sn are presented. It seems that, so far, none of the available theories can adequately interpret our *L*-shell results at low energies. © *2002 American Institute of Physics.* [DOI: 10.1063/1.1470248]

I. INTRODUCTION

The ionization of atoms by electron impact is a process of great importance in atomic and molecular physics. An important motivation for the study of inelastic collisions of electrons stems from the ever-increasing need for cross-section data in such diverse fields as radiation physics, plasma physics, atmospheric physics, astrophysics, and electron microscopy. In many of these application areas, absolute cross sections for inner-shell ionization are required over a wide energy region[1–3] in, for example, electron probe microanalysis (EPMA), Auger electron spectroscopy (AES), fusion research, and so on. Such cross sections are also an important theoretical subject. A variety of theoretical treatments, beginning with that of Bethe,[4] have been made in an attempt to describe this process, either in classical or quantum mechanics.

During the past decade, the study of ionization cross sections of atomic inner shells by electron impact has been of growing interest both experimentally[5–14] and theoretically.[6,15,16] Generally three techniques have been used to measure inner-shell ionization cross sections for both gaseous and solid targets. With one technique, measurements are made of electron energy-loss spectra associated with excitation of the electrons from a particular shell. For the other two techniques, measurements are made of the decay products, either of characteristic x rays or Auger electrons. The latter two approaches are of particular value since data on the cross sections for the yields of x rays or Auger electrons, relevant to EPMA and AES, respectively, are acquired directly.[2] According to the compilations of Liu *et al.*[17] and Joy,[18] experimental inner-shell ionization cross sections by electron impact are still relatively scarce, especially in the low-energy region (i.e., $U \leqslant 4$, where U is the reduced energy defined as the ratio between the incident electron energy and the inner-shell ionization energy), and discrepancies among these data from different measurements for some atoms are apparent. Furthermore, most of the data are for *K*-shell ionization, and the situation with *L* and higher shell is far from satisfactory. The increasing complexities of the multiple decay channels following *L*- and higher-shell ionization are largely responsible for the more limited data for relevant inner-shell ionization cross sections as well as the associated fluorescence yields and the Auger and Coster–Kronig transition probabilities. These complexities are also responsible for the generally poorer accuracy of the measured *L*- and higher-shell cross sections compared to *K*-shell data.

In recent years, Luo *et al.* have made major progress in cross-section measurements in the low-energy region.[8–14] Thin targets with thick substrates were utilized in their experiments, and corrections for the effects of the electrons reflected from thick substrates were made based upon an electron transport calculation.[19] Their method has the advantage of avoiding the difficulties of preparing uniform self-supporting thin targets, and has been applied to measure *K*-shell ionization cross sections for some atoms.[8–14]

[a)]Author to whom correspondence should be addressed; electronic mail: c.h.tang@263.net

TABLE I. Relevant constants for the calculation of Ge *K*-shell ionization cross sections (*Z*: atomic number; *A*: atomic weight; ω_k: *K*-shell fluorescence yield; E_k: *K*-shell ionization energy; I_α/I_β: ratio of $K\alpha$ and $K\beta$ x-ray intensities; ρd: mass thickness of target).

Element	Z	A	ω_k	E_k (keV)	I_α/I_β	ρd (μg/cm^2)
Ge	32	72.59	0.540	11.104	0.147	32.7

In this article, we employ the same method to measure *K*-shell ionization cross-sections σ_K of germanium and extend the method to measurements of absolute cross sections for *L*-shell producing x rays, $\sigma_{L\alpha}$ and $\sigma_{L\beta}$ of tin. Ge and Sn were selected since there are some experimental data in part of our measured energy region. This article aims at checking the existing data and providing new data for practical applications. The experimental data, for energies from near threshold to 40 keV for Ge and for energies from near threshold to 25 keV for Sn, are reported. Comparisons are made of the experimental results with previous measurements and some empirical and theoretical results.

II. EXPERIMENT

A detailed description of the present experimental setup has been given elsewhere,[9,11] and here only a brief description is presented. The experimental setup is identical to one we used earlier.[11] The monoenergetic electron beam from near threshold to 40 keV was provided by an electron gun and adjusted in accordance with the x-ray counting rate; the energy of the incident electron beam was determined by the end point of the obtained bremsstrahlung spectrum. With this method, the incident electron energy could be measured within an uncertainty of 0.1 keV. The electron beam was well collimated and then hit the target, which was placed at 45° with respect to the direction of the incident beam. A horizontal Si(Li) detector was kept inside the vacuum chamber to reduce energy loss from air and was about 10 cm from the center of the target. The detector full width at half maximum was 170 eV for ^{55}Mn $K\alpha$ x rays. The detector efficiency was calibrated with a set of standard radioactive sources, i.e., ^{241}Am, ^{137}Cs, ^{55}Fe, and ^{54}Mn, provided by the China Institute of Atomic Energy. The uncertainty of the calibrated efficiency was believed to be less than 5%. All charges of the incident electron beam were collected by a deep Faraday cup and were led to a digital current integrator. The current integrator was calibrated by a standard current before measurement and its uncertainty was found to be less than 0.3%.[20]

The targets used in our experiments were prepared by evaporating Ge or tin directly onto an aluminum substrate. The film mass thicknesses were determined by weighing, using a balance with a precision of 10^{-6} g. The target thicknesses of Ge and Sn are listed in Tables I and II, respectively. The uncertainty of these values should be less than 10%.[20]

TABLE II. Relevant constants for the calculation of tin *L*-shell x-ray production cross sections (*Z*: atomic number; *A*: atomic weight; E_{Li}: *L*-subshell ionization energy; ρd: mass thickness of target).

Element	Z	A	E_{L1} (keV)	E_{L2} (keV)	E_{L3} (keV)	ρd (μg/cm^2)
Sn	50	118.69	4.456	4.156	3.929	9.4

III. RESULTS AND ANALYSIS

Through the known Ge fluorescence yield ω_K, Ge *K*-shell ionization cross-sections, σ_K, have been deduced from $K\alpha$ x-ray production cross-sections, $\sigma^x{}_{K\alpha}$. For Sn, we present *L*-shell x-ray production cross sections, which can be converted to corresponding *L*-shell ionization cross sections with knowledge of the relevant fluorescence yields.[21] Conversion is quite straightforward but involves a set of atomic parameters, which presently have quite high experimental errors (5%–20%),[22] so no effort has been made to convert the measured *L*-shell x-ray production cross sections to corresponding ionization cross section data. In order to compare our results with the predictions of theories, the *L*-subshell ionization cross sections (σ_{L1}, σ_{L2}, and σ_{L3}) obtained from theoretical calculations must be converted into x-ray production cross sections ($\sigma_{L\alpha}$, $\sigma_{L\beta}$, and $\sigma_{L\gamma}$). A number of literature sources are presently available. The most common sources are: Krause,[22] Chen, Gasemann, and Mark[23] and Puri *et al.*[24] for fluorescent and Coster–Kronig yields and Scofield's tabulations for x-ray emission rate.[25] In this article, the fluorescence yields and Coster–Kronig yields given by Krause are used in order to compare with the results of Baxter and Spicer[26] who used the same parameters to convert theoretical ionization cross sections to x-ray production cross sections.

The x-ray production cross sections $\sigma^x{}_i$ ($i=K_\alpha,L_\alpha,L_\beta,L_\gamma$) are related to the observed x-ray counts $N^x{}_i$ ($i=K_\alpha,L_\alpha,L_\beta,L_\gamma$) by the formula

$$\sigma_i^x=\frac{4\pi N_i^x\cos\theta}{N_e dn\eta\Omega}\quad (i=k_\alpha,L_\alpha,L_\beta,L_\gamma), \tag{1}$$

where n (in atom/cm^3) and d (in cm) are the atomic density and thickness of the target, respectively, N_e is the number of electrons hitting the target, $\eta\Omega/4\pi$ refers to the total detection efficiency for characteristic x rays, and θ denotes the angle between the incident electron beam and the normal at the target surface.

Due to the existence of a thick substrate, reflected electrons, whose energy exceeds the ionization threshold of target atoms, can induce additional inner-shell ionizations of the target atoms, resulting in a systematic overestimation of the cross sections; corrections should be made for this effect. We have calculated the fraction of ionization events caused by electrons reflected from the aluminum substrate. The final expression for x-ray production cross sections can be written as[9]

$$\sigma_i^x(E)=\frac{4\pi N_i^x\cos\theta}{N_e dn\eta\Omega}-\cos\theta\int_{E_i}^{E}\Phi_{\mathrm{ref}}(E')\sigma_i^x(E')dE', \tag{2}$$

where the subscript i indicates K_α, L_α, L_β, L_γ and the second term indicates the fraction of ionization events caused by electrons reflected from the aluminum substrate.

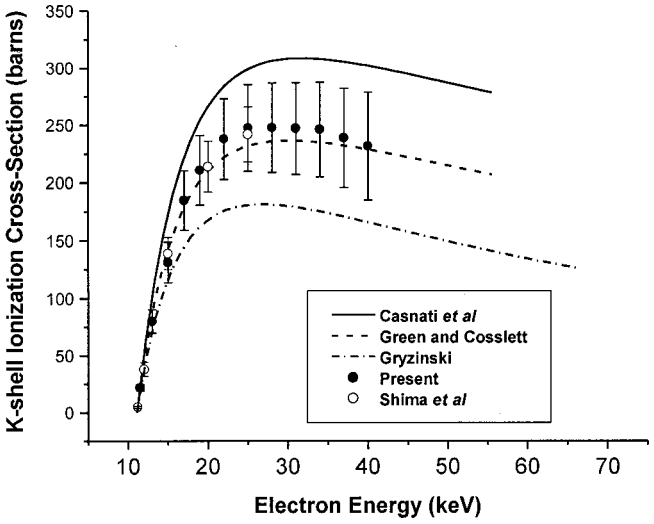

FIG. 1. Ge *K*-shell ionization cross-sections σ_K as a function of electron energy. The solid circles represent the present results. Shima's data are shown by open circles (see Ref. 28). The solid line exhibits the results of the empirical formula of Casnati, Tartari, and Baraldi (see Ref. 31). The dashed line represents the results of the semiempirical formula of Green and Cosslett (see Ref. 30). The results of Gryzinski's formula are denoted by a dot-dashed line (see Ref. 29).

Φ_{ref}, the reflected energy spectrum, is calculated by using the so-called bipartition model of electron transport.[19] Equation (2) can be solved by iteration.

For Ge, the *K*-shell ionization cross-sections σ_K can be expressed in the form

$$\sigma_K = \frac{\sigma_{K\alpha}^{x}}{\omega_K}\left(1+\frac{I_\beta}{I_\alpha}\right), \tag{3}$$

where ω_K is the Ge *K*-shell fluorescence yield, and I_α and I_β refer to the K_α and K_β x-ray intensities, respectively. The relevant parameters used for calculation of σ_K are taken from Ref. 27 and listed in Table I.

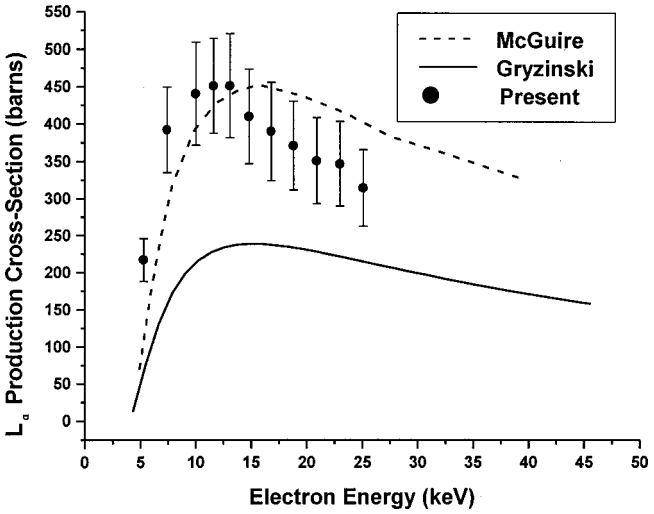

FIG. 2. Sn *L*-shell x-ray production cross-sections $\sigma_{L\alpha}$ as a function of electron energy. The solid circles represent the present results. The solid line represents predictions of Gryzinski's theory (see Ref. 29). Results calculated from McGuire's theory are shown by a dashed line (see Ref. 38).

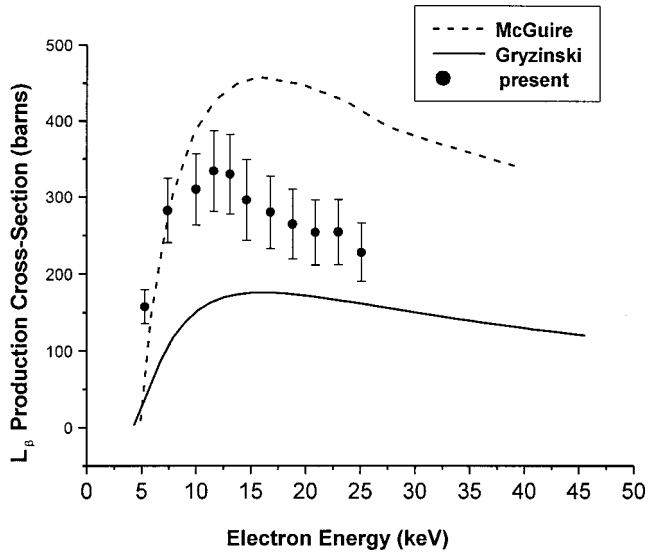

FIG. 3. Sn *L*-shell x-ray production cross-sections $\sigma_{L\beta}$ as a function of the electron energy. The symbols are the same as those in Fig. 2.

The measured *K*-shell ionization cross sections of Ge are plotted in Fig. 1. The *L*-shell x-ray production cross-sections $\sigma_{L\alpha}$ and $\sigma_{L\beta}$ of tin are plotted in Figs. 2 and 3, respectively, and the $\sigma_{L\alpha}/\sigma_{L\beta}$ ratio is plotted in Fig. 4. Unfortunately, L_γ data for Sn could not be analyzed since the L_γ peak was too weak to be distinguished from the background. All of the present experimental results are listed in Table V. Errors mainly arise from counting statistics for the net peak counts (1%–5%), detector efficiency (5%), fluorescence yields (*K*-shell, 3%; *L*-shell, 10%–20%, if conversion is made to *L*-shell ionization cross-sections), target thickness (10%), and inhomogeneity of the targets (3%). Therefore, the total uncertainty (one standard deviation) is estimated to be less than 15%.

In Fig. 1, the present data as well as Shima's data[28] for Ge are shown and compared with the theoretical results of

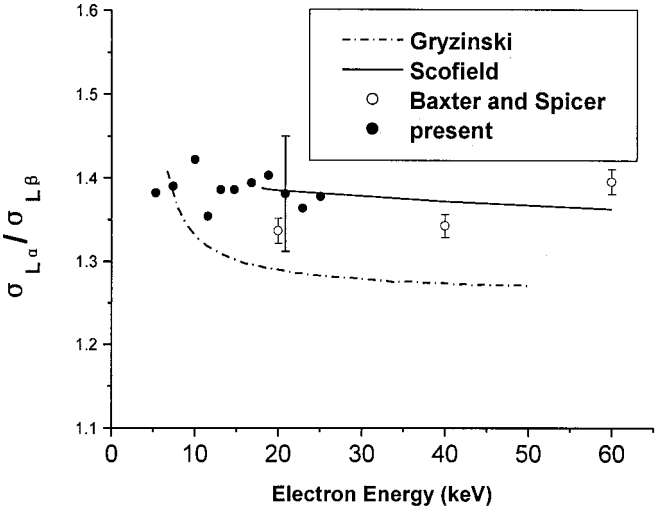

FIG. 4. Measured experimental x-ray intensity ratios $\sigma_{L\alpha}/\sigma_{L\beta}$ for Sn (full circles) are compared with the data of Baxter and Spicer (see Ref. 26). (open circles) as well as with theoretical calculations based on the RBA (see Ref. 25) (solid line) and the BEA (see Ref. 29) (dot-dashed line), respectively.

TABLE III. X-ray emission rates (Γ) for tin.[a]

Γ_1	Γ_2	Γ_3	$\Gamma_{3\alpha}$	$\Gamma_{3\beta}$	$\Gamma_{2\beta}$	$\Gamma_{2\gamma}$	$\Gamma_{1\beta}$	$\Gamma_{1\gamma}$
0.1066	0.1786	0.1696	0.1456	0.018 46	0.1545	0.019 67	0.088 04	0.017 65

[a]See Reference 39.

Gryzinski,[29] and results from the semiempirical formula of Green and Cosslett[30] and the empirical formula of Casnati, Tartari, and Baraldi[31] It can be seen that the present results are in good agreement with Shima's data and with results of the semiempirical formula of Green and Cosslet. The predictions of the empirical formula of Casnati and co-workers overestimate the data and the theoretical results of Gryzinski underestimate the experimental data. Powell has made a comparison[32] of several widely used empirical formulas (i.e., of Casnati and co-workers, Jakoby, Gerg, and Richter,[33] and Deutsch Margreiter and Mark[34]) and of some theoretical results (i.e., of Gryzinski, Khare, and Wadehra[35] and Luo[36]) with experimental *K*-shell ionization cross sections for C, N, O, Ne, Al, Ar, Fe, Ni, Cu, Mo and Ag. He found that the empirical formula of Casnati and co-workers was superior to the others listed above. Based on the measurements in the latest decade,[5,8–13,28,37] we find that the results, given by Green and Cosslett,[30] are closer to the experimental data for medium Z atoms (i.e., $19 \leqslant Z \leqslant 40$) in the low-energy region (i.e., $1 < U < 4$) in which the equation of Bethe[4] is thought to be invalid.

In Figs. 2 and 3, the measured Sn *L*-shell x-ray production cross-sections $\sigma_{L\alpha}$ and $\sigma_{L\beta}$ are compared with two different calculations: the so-called binary encounter approximation (BEA) theory of Gryzinski[29] and the theory of McGuire for atomic rearrangement.[38] For comparison with the experimental data, the *L*-shell ionization cross sections (σ_{L1}, σ_{L2}, and σ_{L3}) obtained from theoretical calculations must be converted into x-ray production cross sections ($\sigma_{L\alpha}$, $\sigma_{L\beta}$ and $\sigma_{L\gamma}$). The relation between *L*-shell ionization cross section and x-ray production cross section can be found in Ref. 21. The x-ray emission rate, and the fluorescence and Coster–Kronig yields used in the conversion calculation for the x-ray production cross sections are listed in Tables III and IV, respectively. In the conversion calculation, we have omitted the negligible contributions of *L*-shell vacancies created in filling *K*-shell vacancies by *L*-shell electrons. It can be seen from Figs. 2 and 3 that the present experimental results generally lie between the predictions of McGuire and of Gryzinski. The shape of the energy dependence of the measured production cross sections is similar to that of Gryzinski, namely, the maximum datum of the cross sections appears at or near $U=3$. However, the Gryzinski values are only about half of the experimental results. The values given by McGuire's theory are closer to the experimental data, although his peak position appears near $U=4$.

Since the errors in the x-ray production cross sections come mainly from the determination of target thickness and detector efficiency, the relative line intensities can be determined with higher accuracy. In Fig. 4, the measured $\sigma_{L\alpha}/\sigma_{L\beta}$ intensity ratios are plotted and compared with results of Baxter and Spicer[26] as well as with the theoretical data of Gryzinski[29] and Scofield.[25] Baxter and Spicer measured the ratios $\sigma_{L\alpha}/\sigma_{L\beta}$ in the energy range from 20 to 100 keV. However, we measured these ratios from near threshold to 25 keV. It can be seen from Fig. 4 that our ratios are in good agreement with Baxter's results in the energy region of overlap (within our 5% experimental error at 20.9 keV).

Using the relativistic form of the first-order Born approximation (RBA), Scofield[25] calculated ionization cross sections down to only 50 keV, similar to the range of the results of Baxter and Spicer.[26] An extrapolation based upon Scofield's polynomial fit was performed to enable comparisons with our data near 20 keV. We can see from Fig. 4 that the extrapolation of Scofield's theory is in reasonable agreement with our results. For the near-threshold results, the discrepancies are obvious in that there are different trends of the $\sigma_{L\alpha}/\sigma_{L\beta}$ ratios as a function of incident electron energy between the experimental data and the predictions from the binary encounter approximation (BEA) theory of Gryzinski.

In conclusion, we have reported experimental *K*-shell ionization cross sections of Ge and absolute *L*-shell x-ray production cross sections of Sn. For the *K*-shell ionization cross sections, our experimental data for medium Z at low energies ($1 < U < 4$) can be reproduced well by the semiempirical formula of Green and Cosslett. For the *L*-shell

TABLE IV. Fluorescence yields (ω_i) and Coster–Kronig transition probabilities (f_{ij}) for tin.[a]

Constants	ω_1	ω_2	ω_3	f_{12}	f_{13}	f_{23}
Values	0.037	0.065	0.064	0.17	0.27	0.157
Uncertainties (%)	20	10	10	20	15	20

[a]See Reference 22.

TABLE V. Measured Ge *K*-shell ionization cross-sections σ_K and Sn *L*-shell x-ray production cross-sections $\sigma_{L\alpha}$ and $\sigma_{L\beta}$ by electron impact. (E_i refers to incident electron energy; the numbers in parentheses refer to total estimated one-standard-deviation uncertainty).

E_i	Ge	E_i	Sn	
(keV)	σ_K (barn)	(keV)	$\sigma_{L\alpha}$ (barn)	$\sigma_{L\beta}$ (barn)
11.5	22.0(±2.9)	5.3	217.0(±28.8)	157.7(±21.9)
13.0	79.9(±10.2)	7.4	392.3(±57.2)	282.3(±42.0)
15.0	131.4(±17.6)	10.0	440.5(±68.7)	309.8(±46.7)
17.0	184.8(±25.4)	11.6	451.2(±63.4)	333.9(±53.0)
19.0	210.8(±30.0)	13.1	451.1(±69.5)	329.8(±52.5)
22.0	238.0(±35.1)	14.6	410.2(±63.3)	296.0(±52.6)
25.0	247.6(±37.7)	16.8	390.1(±66.2)	279.9(±47.2)
28.0	247.8(±39.0)	18.8	371.1(±59.4)	264.6(±45.3)
31.0	247.1(±39.9)	20.9	350.7(±57.7)	253.9(±42.2)
34.0	246.3(±41.2)	23.0	346.7(±56.9)	254.3(±42.4)
37.0	239.0(±43.4)	25.1	314.1(±51.7)	228.0(±37.8)
40.0	231.7(±46.8)			

data, it seems that, so far, none of the available theories can adequately interpret our *L*-shell results at low energies. Further investigation is needed, both experimentally and theoretically, for a better understanding of the inner-shell ionization processes.

ACKNOWLEDGMENTS

This work was supported by the National Natural Science Foundation of China under Grant No. 19874045 and by the Key Project of the Education Ministry of China.

[1] C. J. Powell, Rev. Mod. Phys. **48**, 33 (1976).
[2] C. J. Powell, *Electron Impact Ionization*, edited by T. D. Mark and G. H. Dunn (Springer, New York, 1985), Chap. 6.
[3] C. J. Powell, in *Microbeam Analysis-1990,* edited by J. R. Michael and P. Ingram (San Francisco Press, San Francisco, 1991), p. 13.
[4] H. Bethe, Ann. Phys. (Leipzig) **5**, 325 (1930).
[5] V. P. Shevelko, A. M. Solomon, and V. S. Vukstich, Phys. Scr. **43**, 158 (1991).
[6] H. Schneider, I. Tobehn, E. F. Tobehn, and R. Hippler, Phys. Rev. Lett. **71**, 2707 (1993).
[7] R. Shanker and R. Hippler, Z. Phys. D: At., Mol. Clusters **42**, 161 (1997).
[8] Z. An, T. H. Li, L. M. Wang, and Z. M. Luo, Phys. Rev. A **54**, 3067 (1996).
[9] Z. M. Luo, Z. An, F. Q. He, T. H. Li, X. G. Long, and X. F. Peng, J. Phys. B **29**, 4001 (1996).
[10] Z. M. Luo, Z. An, T. H. Li, L. M. Wang, Q. Zhu, and X. Y. Xia, J. Phys. B **30**, 2681 (1997).
[11] F. Q. He, X. G. Long, X. F. Peng, Z. M. Luo, and Z. An, Nucl. Instrum. Methods Phys. Res. B **114**, 213 (1996); **129**, 445 (1997).
[12] X. F. Peng, F. Q. He, X. G. Long, Z. M. Luo, and Z. An, Phys. Rev. A **58**, 2034 (1998).
[13] C. H. Tang, Z. M. Luo, Z. An, and T. H. Li, Chin. Phys. Lett. **16**, 505 (1999).
[14] X. F. Peng, F. Q. He, X. G. Long, Z. An, and Z. M. Luo, Chin. Phys. Lett. **18**, 39 (2001).
[15] S. P. Khare and J. M. Wadehra, Can. J. Phys. **74**, 376 (1996).
[16] S. Luo, Ph.D. thesis, The University of Tennessee, Knoxville, (1994); S. Luo and D. C. Joy, in Microbeam Analysis-1991, edited by D. G. Howitt (San Francisco Press, San Francisco, 1991), p. 67.
[17] M. T. Liu, Z. An, C. H. Tang, Z. M. Luo, X. F. Peng, and X. G. Long, At. Data Nucl. Data Tables **76**, 213 (2000).
[18] D. C. Joy, Scanning **17**, 270 (1995).
[19] Z. M. Luo, Phys. Rev. B **32**, 812 (1985); **32**, 824 (1985).
[20] C. H. Tang, Ph.D. thesis, Sichuan University, Chengdu, 2000, P. R. China.
[21] J. Palinkas and B. Schlenk, Z. Phys. A **297**, 29 (1980).
[22] M. O. Krause, J. Phys. Chem. Ref. Data **8**, 307 (1979).
[23] M. H. Chen, B. Crasemann, and H. Mark, Phys. Rev. A **24**, 177 (1981).
[24] S. Puri, D. Mehta, B. Chand, N. Singh, and P. N. Trehan, X-Ray Spectrom. **22**, 358 (1993).
[25] J. H. Scofield, Phys. Rev. A **18**, 963 (1978).
[26] G. W. Baxter and B. M. Spicer, Aust. J. Phys. **36**, 287 (1983).
[27] Y. Z. Liu, *Decay Scheme of the Usual Radioisotopes* (Atomic Energy, Beijing, 1982) (in Chinese).
[28] K. Shima, T. Nakagawa, K. Umetani, and T. Mikumo, Phys. Rev. A **24**, 72 (1981).
[29] M. Gryzinski, Phys. Rev. **138**, A336 (1965).
[30] M. Green and V. E. Cosslett, Proc. Phys. Soc. London **78**, 1206 (1961).
[31] E. Casnati, A. Tartari, and C. Baraldi, J. Phys. B **15**, 155 (1982).
[32] C. J. Powell (private communication).
[33] C. Jakoby, H. Genz, and A. Richter, J. Phys. Colloq. **48**, 487 (1987).
[34] H. Deutsch, D. Margreiter, and T. D. Mark, Z. Phys. D: At., Mol. Clusters **29**, 31 (1994).
[35] S. P. Khare and J. M. Wadehra, Can. J. Phys. **74**, 376 (1996).
[36] S. Luo, Ph.D. Thesis, University of Tennessee, 1994; S. Luo, and D. C. Joy, *Microbeam analysis-1991*, edited by D. G. Howitt (San Francisco Press, San Francisco, 1991).
[37] Z. An, C. H. Tang, C. G. Zhou, and Z. M. Luo, J. Phys. B **33**, 3677 (2000).
[38] E. J. McGuire, Phys. Rev. A **16**, 73 (1977).
[39] J. H. Scofield, At. Data Nucl. Data Tables **14**, 121 (1974).